Cochlear Implantation of Slim Precurved Arrays Using Automatic Preoperative Insertion Plans

*Kareem O. Tawfik, †Mohammad M.R. Khan, *Ankita Patro, ‡Miriam R. Smetak, *David Haynes, §Robert F. Labadie, ||René H. Gifford, and *¶Jack H. Noble

**Department of Otolaryngology–Head & Neck Surgery, Vanderbilt University Medical Center, Nashville, Tennessee; †Department of Computer and Data Science, Meharry Medical College, Nashville, Tennessee; ‡Department of Otolaryngology–Head & Neck Surgery, Washington University School of Medicine, St. Louis, Missouri; §Department of Otolaryngology–Head & Neck Surgery, Medical University of South Carolina, Charleston, South Carolina; ||Hearts for Hearing, Oklahoma City, Oklahoma; and ¶Department of Electrical & Computer Engineering, Vanderbilt University, Nashville, Tennessee*

Hypothesis: Preoperative cochlear implant (CI) electrode array (EL) insertion plans created by automated image analysis methods can improve positioning of slim precurved EL.

Background: This study represents the first evaluation of a system for patient-customized EL insertion planning for a slim precurved EL.

Methods: Twenty-one temporal bone specimens were divided into experimental and control groups and underwent cochlear implantation. For the control group, the surgeon performed a traditional insertion without an insertion plan. For the experimental group, customized insertion plans guided entry site, trajectory, curl direction, and base insertion depth. An additional 35 clinical insertions from the same surgeon were analyzed, 7 of which were conducted using the insertion plans. EL positioning was analyzed using postoperative imaging autosegmentation techniques, allowing measurement of angular insertion depth (AID), mean modiolar distance (MMD), and scalar position.

Results: In the cadaveric temporal bones, three scalar translocations, including two foldovers, occurred in 14 control group insertions. In the clinical insertions, translocations occurred in 2 of 28 control cases. No translocations or folds occurred in the seven experimental temporal bone and the seven experimental clinical insertions. Among the nontranslocated cases, overall AID and MMD were 401 ± 41 degrees and 0.34 ± 0.13 mm for the control insertions. AID and MMD for the experimental insertions were 424 ± 43 degrees and 0.34 ± 0.09 mm overall and were 432 ± 19 degrees and 0.30 ± 0.07 mm for cases where the planned insertion depth was achieved.

Conclusions: Trends toward improved EL positioning within scala tympani were observed when EL insertion plans are used. Variability in MMD was significantly reduced (0.07 versus 0.13 mm, $p = 0.039$) when the planned depth was achieved.

Key Words: Cochlear implant—Electrode array positioning—Precurved electrode array—Surgical planning.

Otol Neurotol **00:**00–00, 2025.

INTRODUCTION

Cochlear implantation (CI) is a standard treatment approach for individuals experiencing severe-to-profound sensorineural hearing loss or those experiencing moderate low frequency and severe-to-profound high frequency hearing loss (1). CI electrode arrays (ELs) can be broadly divided into two categories: straight and precurved. Precurved ELs are designed to approximate the curvature of the average human cochlea's modiolar wall, allowing for perimodiolar positioning (2,3). The intracochlear positioning of precurved arrays is associated with speech recognition rates (4–8). Location within the scala tympani (ST) is consistently shown to be associated with better audiologic outcomes (4,5,7–9). Close proximity of the electrodes to the modiolus is hypothesized to decrease spread of excitation and has been shown to be associated with better speech recognition outcomes (4–6). Angular insertion depth (AID) of the tip of the array measured relative to the center of the round window has been associated with better speech recognition outcome in some studies, e.g., (10), and worse speech recognition outcomes in others, e.g. (4,5). Precurved arrays are designed to achieve perimodiolar seating at a specific depth. Low AID can result in lack of stimulation in the apical portion

Address correspondence and reprint requests to: Jack H. Noble, Ph.D., Department of Electrical & Computer Engineering, Vanderbilt University, 2301 Vanderbilt Pl., Box 1679, Station B, Nashville, TN 37235; E-mail: jack.noble@vanderbilt.edu

Sources of support and disclosure of funding: K.O.T. has served as an advisory board member for GlaxoSmithKline. D.S.H. is a consultant for Advanced Bionics, Cochlear Americas, MED-EL GmbH, Stryker, Synthes, Grace Medical, and Oticon. R.H.G. is a consultant for Advanced Bionics, Akouos, and Cochlear Americas; is on the clinical advisory board for Frequency Therapeutics; and is on the Board of Directors for the American Auditory Society.

This work was supported in part by NIH Grants R01DC008408 and R01DC014037 from the National Institute on Deafness and other Communication Disorders and UL1TR000445 from the National Center for Advancing Translational Sciences. The content is solely the responsibility of the authors and does not necessarily reflect the views of these institutes.

Mohammad M.R. Khan is a co-first author.

DOI: 10.1097/MAO.0000000000004525

of the cochlea and might result in extracochlear electrodes that do not provide auditory benefit (11). High-AID due to over-insertion could lead to poor perimodiolar seating of the array and potential intracochlear trauma. Thus, a possible reason for the conflicting findings regarding AID is that both high and low AIDs are negatively associated with outcomes.

Although associations between EL positioning and outcomes have been reported in numerous studies, styletted precurved EL have been associated with a high risk of scalar translocation (12) and often do not achieve the intended ideal perimodiolar positioning (13). Variability in EL positioning is not surprising given that cochlear anatomy is variable (14–17). Therefore, precurved EL insertion planning techniques based on patient-specific cochlear anatomy have been proposed to improve EL positioning and patient outcomes (13,18).

One of the main barriers for EL insertion planning is the difficulty in accurately segmenting cochlear anatomy due to the resolution of available preoperative images. Although tremendous progress has been made in MRI imaging of the ear (19), computed tomography (CT) offers the best resolution and ability to localize key landmarks used by surgeons such as the chorda tympani (20). Yet, visualization of intracochlear structures such as the scala tympani (ST), scala vestibuli (SV), and modiolus can be challenging with CT. Previously published auto-segmentation techniques use a high-resolution micro-CT (μCT) nonrigid cochlear atlas (21–23) to infer the position of fine structures of patients' cochleae that cannot be resolved with clinical CT with high accuracy. Other groups have developed synchrotron-based atlases but have not developed approaches to nonrigidly register them to in vivo patient CTs (24).

A novel method to create patient-specific insertion trajectories using similar segmentation techniques to identify intracochlear anatomy as well as the facial nerve, chorda tympani, and ossicles has been evaluated (18,25,26). Previous temporal bone insertion experiments with the Advanced Bionics (Valencia, CA) Mid-Scala electrode showed statistically significant improvement in EL positioning within the ST when insertion planning was used (18). In the current study, we compared EL positioning with and without CT-based insertion planning for a slim precurved EL by an experienced attending surgeon who was inexperienced with CT-based insertion planning methods, in order to evaluate whether the planning approach is effective for another EL and surgeon.

METHODS

Experimental Protocol

Twenty-one cadaveric temporal bone specimens were used. Each cochlea was implanted with a slim precurved EL (CI532/632; Cochlear Americas, Centennial, CO) by a surgeon who was experienced with this EL. The bones were evenly divided into three groups: experimental group (Exp), control group 1 (C1), and control group 2 (C2). To measure baseline performance in EL positioning, the C1 group was implanted without insertion plans. Next, the Exp group was implanted using customized EL insertion plans designed using preoperative cone-beam CT. Plans were created using an extended version of the previously described approach (18). The plan included instructions on insertion trajectory (pitch, yaw, and roll) and insertion depth. Last, the C2 group was implanted without insertion planning to detect potential changes in surgical technique after exposure to insertion planning.

After institutional review board approval, an analysis of patients who underwent cochlear implantation with a slim precurved EL by the same surgeon without custom insertion plans was conducted. After removing subjects for whom there were cochlear abnormalities, such as ossification or malformations, as well as revision surgeries, 28 implanted ears from 25 patients were identified with pre- and postoperative CT scans for analysis. Additionally, seven ears of seven patients were implanted by the same surgeon using customized EL insertion plans in a period of time ranging from 4 to 15 months after the completion of the temporal bone implantations. A clinical database was used to determine demographic information for the 32 patients as well as word recognition rates at least 6 months after implantation. Word recognition rates were assessed using the Consonant-Nucleus-Consonant (CNC) word recognition test (50-word list presented at 60 dB SPL) (27). Test scores were collected as part of clinical routine in the unilateral, electric-only listening condition, as well as the bimodal (CI + contralateral hearing aid) condition for bimodal listeners. Of the 35 implanted ears, scores were available for 17 ears. If scores from more than one time point were available, the maximum score was recorded.

Electrode Insertion Planning

Previously published techniques were used to create customized EL insertion plans based on preoperative CT imaging (18). In brief, 1) measurements of the EL were used to create a model that represents the resting-state shape of the EL; 2) the structures of interest, including the ST, facial nerve, chorda, and ossicles, were automatically segmented in the preoperative CT scan; 3) the array model was automatically registered, i.e., aligned, to the patient's ST modiolar wall to determine the positioning of the EL that would achieve ideal seating of the EL against the patient's modiolus (an example result is shown in Fig. 1D); and 4) insertion angles (roll, pitch, yaw) and depth (referenced to the 3 white markers placed by the manufacturer at the base of the EL) were determined to match the positioning of the registered array model.

This method was modified to add an over-insertion, followed by pull-back technique (28). The base insertion depth was defined as the distance of the middle depth marker on the array to the point where the RW plane and the insertion vector intersect (see Fig. 1D). An initial over-insertion to a depth of 2 mm beyond the recommended final array model base insertion depth was recommended, followed by pull-back of the array until the planned base insertion depth was achieved. This technique has been shown to achieve a more perimodiolar position of the EL compared with simply stopping at the planned depth without additional manipulation (28,29). Although AID was not reported in (28), we hypothesized that the pull-back technique should also lead to achieving more ideal AID. The

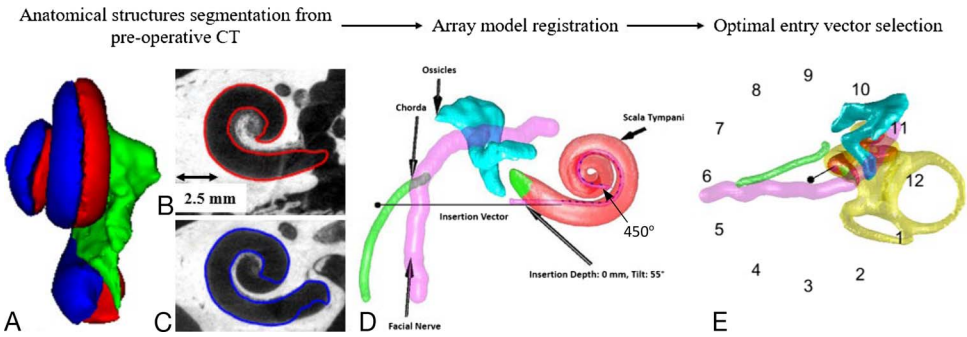

FIG. 1. The steps for the proposed EL insertion planning system are shown. *A*, The intracochlear cavity atlas surface models are shown. *B* and *C*, Superimposed contours on one of the microCT atlases are shown. *D*, A model of the EL aligned with the medial wall of the automatically segmented ST is shown. *E*, The selected optimal trajectory (black line) for a substantially extended RW entry site is shown.

slim precurved array is designed to achieve good fit to the modiolus at approximately 450-degree AID because the resting shape of the array curls is approximately 450 degrees into the cochlea (as can be observed in Fig. 1D).

In each case, three solutions were generated that corresponded to three different cochlear entry points: middle of the round window, a slightly extended round window, and a substantially extended round window. From the three optional plans, the surgeon selected the insertion plan that was most feasible with the given anatomy. An example of a selected insertion plan entry vector is shown in Figure 1E. In this example, the optimal trajectory, which uses a substantially extended round window and is collinear with the ST base, takes a path that is closer to the facial nerve than the chorda.

The insertion plan was presented to the surgeon in both an interactive 3D rendering (Fig. 2) and a simple text format with reference to structures that can be visualized directly. The following is an example of plan instructions in text format:

The curl direction and the insertion point were presented as a clock-face position. The EL insertion site was presented with a clock face centered at the RW center and using the stapes footplate as the 12:00 reference angle (Fig. 2A). For determining curl direction, the center of the stapes footplate served as the 12:00 reference angle with the center of the clock face at the EL entry site (Fig. 2B).

Analysis

Postoperative cone-beam CT was used to evaluate the EL position using previously reported automated methods (30,31). Scalar location; mean modiolar distance (MMD); defined as the average distance from the center of each contact to the closest point on the modiolar wall; apical mean modiolar distance (AMD), defined as the average distance from the most apical 11 contacts to the closest point on the modiolar wall; and the angular insertion depth (AID) for each EL were measured. EL position was recorded twice for the experimental temporal bones, once before pullback via cone-beam CT, then again after pullback via a subsequent CT.

Effectiveness of EL insertion planning in improving EL placement was determined by comparing key markers of EL positioning in the C1 and Exp specimen groups. The C2 group was used to measure whether the planning method led to changes in surgical technique. Similarly, scalar location, MMD, AMD, and AID were used to measure the effectiveness of insertion plans in the clinical dataset compared with control cases where no plan was used. To analyze the impact of experimental plans when array folding or translocation does not occur, summary EL position statistics for MMD, AMD, and AID were conducted while leaving out folded and translocated cases. As the Kolmogorov-Smirnov test indicated non-normality of EL position metrics, statistically significant

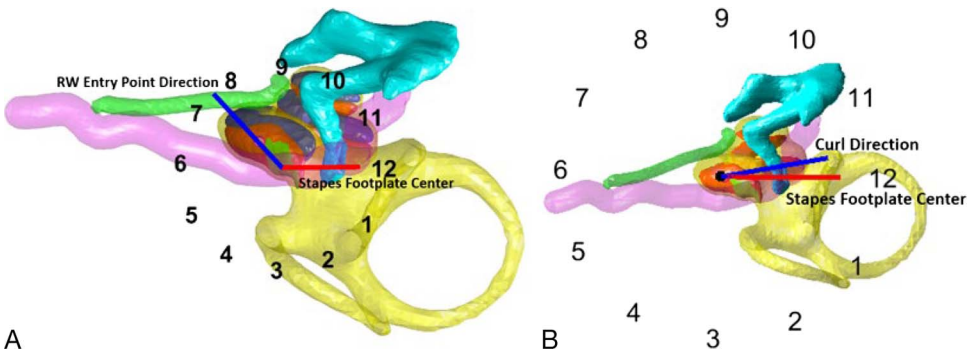

FIG. 2. *A*, Clock-face representation of the entry site location relative to the center of the RW. The center of the stapes footplate defines 12:00, and the center of the clock face is the RW center. *B*, Clock-face representation of the array curl direction. The center of the stapes footplate defines 12:00. The center of the clock face is the EL entry site while viewing down the selected trajectory.

Entry site: Substantially extended RW

Insertion vector: Distance of the insertion trajectory from the facial nerve: 1.5 mm. Distance of the insertion trajectory from the chorda: 0.5 mm. Distance of the insertion trajectory from the ossicles: 3 mm. Tilt of the optimal trajectory with the round window plane (0 degrees indicates perpendicular insertion): 55 degrees. Curl direction (considering clock-face centered on the entry site and the stapes footplate is at 12 o'clock): 11:30. Round window insertion site (considering clock-face centered on middle of round window and the stapes footplate is at 12 o'clock): 07:30

Base insertion depth: The proximal (closest to the surgeon) marker should be inserted until it is 1.5 mm past the entry point.

Pullback: After the array is inserted with the proximal (closest to the surgeon) marker 1.5 mm inside the entry point, then pullback the array until the middle marker is 0.5 mm outside the entry point.

differences between specimen group or patient group means were assessed using Mann-Whitney *U* tests with a threshold of $p < 0.05$. Paired *t* tests with a threshold of $p < 0.05$ were used to assess statistically significant differences within the experimental specimen group across the before and after pullback conditions. Brown-Forsythe variation tests with a threshold of $p < 0.05$ were used to assess differences in variation across groups.

For the experimental groups, the difference between the recommended final depth of the middle marker and the actual final depth of the middle marker measured using post-implant CT, which we refer to as "base depth error," was recorded. The depth error indicates how well the planned final insertion depth was achieved. In the prior work, it was found that smaller depth errors were significantly associated with better MMD and that depth errors less than 1.5 mm tended to be sufficient to lead to good placement (18). Therefore, in addition to comparing the full experimental group to the control cases, we also perform a comparison of the subgroup of experimental cases where the absolute base depth error was less than 1.5 mm. This analysis is useful to understand how EL positioning could be improved if improvements were made to the system to provide the surgeon active feedback on EL positioning.

RESULTS

Temporal Bone Study

Individual specimen EL position analysis results for each test group are presented in Table 1A, and summary statistics are presented in Table 1B. two scalar translocations were observed in C1, where one was also a folded array. One array in C2 translocated and folded. No translocations or folds were observed in the experimental group. Summary EL position statistics on cases without translocations (WT) and folds are shown in the "Control WT" rows. In the bottom of Table 1B, *p* values for statistical comparisons between groups are shown. "Exp versus Control WT" indicates all experimental cases in the Exp group (after pullback) compared with the entire control set (C1 WT and C2 WT combined). The remaining comparisons (Exp versus C1 WT, C1 WT versus C2 WT, and Before Pullback versus Exp) indicate comparisons between these specific groups. As seen in Table 1B, no statistically significant differences were detected for any of the comparisons at the current sample size.

Clinical Study

Individual EL position analysis results for subjects in the clinical database are presented in Table 2A, and summary statistics on EL positioning and word recognition rates are presented in Table 2B. In the bottom of the table, *p* values for statistical comparisons between groups are shown. *"*Cont. WT versus Exp. All*"* indicates all 26 nontranslocated cases in the control group compared with the 7 cases in the entire experimental group. "Before versus Exp. All" indicates a comparison between the 6 control cases implanted before starting the clinical study and the entire experimental group. "Before versus After WT' indicates a comparison between the "Before" and "After" control subgroups without the translocations. No statistically significant difference in average EL positioning was detected with the current sample size.

The first case in the clinical experimental group, subject 6 can be observed to be deeply over-inserted to 542 degrees (see Table 2A). The base insertion depth error in this case was 2.7 mm, indicating that the base of the array was inserted substantially past the planned depth, which likely led to the high AID, MMD, and AMD values. Subject 12 had a base insertion depth error of −2.2 mm, indicating that it is much shallower than the planned depth. The experimental $|D| < 1.5$-mm subgroup reports EL summary statistics when not including these two cases where the actual depth did not well match the planned depth.

In Table 3, results across the temporal bone specimen and clinical cases are pooled, showing average and standard deviation statistics on AID, MMD, and AMD for the 37 control WT cases, 14 experimental cases, and the 11 experimental cases where the absolute base depth error was less than 1.5 mm. In the bottom of the table, *p* values are shown for Mann-Whitney *U* tests and Brown Forsythe variation tests for significant differences between the control and two experimental groups. No significant differences in rank are detected by the Mann-Whitney *U* test at this sample size. The Brown Forsythe test did not detect significance for MMD or AMD, but revealed a significant difference in standard deviation of MMD between the control WT and the experimental group with depth error less than 1.5 mm.

Scatter plots with correlation regression lines are shown in Figure 3 comparing AID error in degrees (assuming an ideal depth of 450 degrees) with CNC word scores in panel A, MMD with CNC word scores in panel B, and AMD with CNC word scores in panel C across all 17 subjects for whom word scores were available. The Pearson correlation coefficient between CNC word scores versus AMD and MMD was found to not be significant at this sample size, with $R = -0.34$ ($p = 0.19$) and $R = -0.37$ ($p = 0.14$). The correlation between AID depth error and CNC word scores was found to be significant with $R = -0.53$ ($p = 0.03$).

DISCUSSION

Precision medicine has opened a new dimension in the healthcare system. However, due to the traditional one-

TABLE 1. *Electrode position analysis results for each specimen in the temporal bone study (A) and summary statistics for each condition and group (B)*

(A)

Specimen	Condition	Group	*D* (mm)	Scalar Location	Fold	AID (°)	MMD (mm)	AMD (mm)
1	Control	C1		ST/SV	N	336	0.63	0.61
2				ST	N	459	0.22	0.13
3				ST	N	435	0.14	0.13
4				ST	N	429	0.31	0.07
5				ST	N	430	0.25	0.12
6				ST/SV	Y	199	0.83	0.75
7				ST	N	387	0.32	0.22
8	Experimental	Before pullback		ST	N	428	0.30	0.07
9				ST	N	438	0.39	0.23
10				ST	N	443	0.41	0.23
11				ST	N	416	0.47	0.36
12				ST	N	357	0.30	0.18
13				ST	N	416	0.33	0.14
14				ST	N	434	0.19	0.16
8		After pullback (Exp)	−1.20	ST	N	441	0.28	0.09
9			−1.10	ST	N	412	0.35	0.12
10			−1.30	ST	N	416	0.40	0.20
11			−0.50	ST	N	425	0.34	0.22
12			−1.70	ST	N	342	0.39	0.18
13			−0.30	ST	N	409	0.40	0.16
14			−0.70	ST	N	426	0.19	0.11
15	Control	C2		ST	N	322	0.48	0.48
16				ST	N	431	0.26	0.40
17				ST	N	438	0.18	0.10
18				ST/SV	Y	188	1.01	0.88
19				ST	N	374	0.44	0.12
20				ST	N	425	0.32	0.20
21				ST	N	387	0.37	0.20

(B)

Condition	Group	Scalar Translocations	Folded Arrays	AID (°)	MMD (mm)	AMD (mm)
Control	C1	2	1	382 (84)	0.38 (0.23)	0.29 (0.25)
	C2	1	1	366 (82)	0.44 (0.25)	0.34 (0.26)
Control WT	C1			428 (23)	0.31 (0.15)	0.21 (0.20)
	C2			396 (41)	0.34 (0.10)	0.25 (0.14)
Experimental	Before pullback	0	0	419 (27)	0.34 (0.08)	0.20 (0.08)
	Exp	0	0	410 (30)	0.34 (0.07)	0.15 (0.05)
	Mann-Whitney *U*-test *p* value	Exp versus Control WT		0.5869	0.2976	0.6507
		Exp versus C1 WT		0.1675	0.0618	0.6847
		C1 WT versus *C2* WT		0.2353	0.1207	0.3153
	Paired *t*-test *p* value	Before Pullback versus Exp		0.3151	0.4757	0.1152

(A) Electrode position analysis results for each specimen in the temporal bone study. Each row corresponds to an individual specimen. For the experimental condition specimens, there is a separate row for before and after pullback. For the control conditions, the group (*C1* or *C2*) is listed in the group column. *D* indicates the base depth error. Negative errors indicate the actual depth is shallower than the depth suggested by the plan, and positive errors indicate the actual depth is deeper than the depth suggested by the plan. Scalar location is denoted "ST" for ELs that are entirely within the scala tympani and "ST/SV" for those for which some electrodes translocate to the scala vestibuli (SV). The column "Folded" contains "Y" for ELs that were folded in the cochlea and "N" otherwise. The AID, MMD, and AMD columns report these measurements for each EL. (B) Summary statistics for each condition and group. Counts of the number of ELs that have translocated or folded in each group are shown in the "Scalar translocations" and "Folded array" columns. The AID, MMD, and AMD columns report the mean as well as the standard deviation in parentheses for each measure for each group.

electrode-size-fits-most approach to CI, patient-specific EL insertion planning has yet to come into widespread use. Currently, the average postoperative sentence and word recognition are reported to be between 56 to 70% and 41 to 55% (32–34), respectively. Customized EL insertion planning offers the opportunity to potentially improve postoperative hearing performance with improved EL positioning (5). Indeed, even in this relatively small study, a significant correlation was found between AID error and CNC word scores ($R = -0.53$, $p = 0.03$), as well as a trend toward a correlation between CNC word scores and both AMD and MMD. These data support that techniques that reduce AID errors, AMD, or MMD might improve hearing outcomes.

Herein, we report the results of using customized EL insertion plans, which aim to improve EL positioning, first in a temporal bone specimen study, then in a clinical study. Although we currently are unable to measure how well the surgeon adhered to the planned insertion angles, we can measure the difference, *D*, between the planned and the actual depth of the base of the array relative to the round window measured from post-insertion CT. *D* is reported for each experimental case in Tables 1 and 2. In specimen 12,

TABLE 2. *Electrode position analysis results for each subject (A) and summary statistics for each condition and group (B)*

(A)

Subj	Condition	Side	Dur. HL (yr)	Wear Time (h/d)	Age at Implantation (yr)	Age at Testing (yr)	Hearing Configuration	First Ear	Etiology	Sex	Base Depth Error (mm)	Scalar Location	AID (°)	MMD (mm)	AMD (mm)	CNC Words—Implant Only (%)	CNC Words—Bimodal (%)
1	Cont	L	8	7.7	42	43	Bilat	N	ANSD	F		ST	331	0.15	0.20	50	
2	Cont	R		12.6	79	80	Unil	Y	Noise	M		ST	395	0.43	0.19	74	
3	Cont	L			56		Bimod	Y	Unknown	F		ST	384	0.27	0.11		
4	Cont	L			1		Bilat	Y	Unknown	F		ST	430	0.50	0.23		
4	Cont	R			1		Bilat	Y	Unknown	F		ST	414	0.36	0.17		
5	Cont	R			3		Unil	Y	Unknown	F		ST	376	0.43	0.09		
6	Exp	L	27	15.8	38	39	Bilat	N	Unknown	F	2.7	ST	542	0.58	0.57	22	
7	Exp	L			21		Unil	Y	Meningitis	F	−0.5	ST	451	0.28	0.22		
8	Exp	L	1	14.0	72	73	Bimod	Y	Noise	F	−0.8	ST	445	0.32	0.17	80	80
9	Cont	L		10.2	58	60	Unil	Y	Menière's	F		ST	377	0.50	0.33	58	
10	Exp	R	13	8.1	18	19	Bimod	Y	Unknown	F	0.2	ST	391	0.21	0.25	86	86
11	Exp	R	9	14.2	60	61	Bimod	N	Noise	M	−0.7	ST	423	0.26	0.17	74	82
12	Exp	R		12.5	40		Bilat	Y	Meningitis	F	−2.2	ST	407	0.40	0.07		
13	Exp	L	22	16.6	59	61	Bimod	Y	Menière's	M	0.1	ST	401	0.23	0.30	88	90
14	Cont	R			4		Bilat	Y	Unknown	M		ST	411	0.17	0.17		
15	Cont	L		13.7	82	83	Unil	Y	Noise	M		ST	444	0.22	0.12	70	
16	Cont	L		15.0	28	29	Bimod	Y	Otoscler.	M		ST	318	0.36	0.16	30	72
17	Cont	L			4		Unil	Y	Unknown	M		ST	415	0.55	0.61		
18	Cont	L	31	12.1	36	36	Unil	Y	Unknown	F		ST	363	0.37	0.10	84	
19	Cont	L		14.5	79	79	Unil	Y	Noise	M		ST	407	0.22	0.08	60	
20	Cont	L	20	11.5	69	69	Bimod	Y	Familial	F		ST	442	0.46	0.49	84	80
21	Cont	R			32		Unil	Y	NT2	F		ST/SV	391	0.66	0.67		
22	Cont	L		7.8	19	19	Unil	Y	Unknown	F		ST	388	0.29	0.29	34	
23	Cont	R	66	22.5	70	71	Bilat	N	Unknown	F		ST	348	0.43	0.33	42	
24	Cont	L			6		Bilat	Y	Unknown	M		ST	433	0.13	0.12		
24	Cont	R			6		Bilat	Y	Unknown	M		ST	422	0.43	0.13		
14	Cont	L			5		Bilat	N	Unknown	M		ST	399	0.14	0.18		
25	Cont	R	11	11.2	61	62	Bimod	Y	Noise	M		ST	446	0.38	0.26	52	94
26	Cont	L			46		Bimod	Y	Unknown	M		ST	389	0.38	0.14		
27	Cont	L	55		73		Bimod	Y	Noise	M		ST	447	0.44	0.40		
28	Cont	R			85		Bimod	Y	Noise	M		ST	408	0.31	0.08		
29	Cont	R			70		Bimod	Y	Unknown	F		ST	438	0.17	0.08		
30	Cont	R			45		Bimod	Y	Menière's	F		ST	276	0.65	1.03		
31	Cont	R	15	12.5	79	80	Bimod	Y	Noise	M		ST	403	0.47	0.38	42	78
32	Cont	L			61		Bimod	Y	Menière's	M		ST/SV	290	0.67	0.47		

(B)

Group	Subgroup	Scalar Translocations	AID (°)	MMD (mm)	AMD (mm)	CNC Word Recog. Rate—Implant Only (%)	CNC Word Recog. Rate—Bimodal (%)
Cont.	All (N = 28)	2	392 (45)	0.38 (0.15)	0.27 (0.22)	54.3 (18.76), N = 12	81.0 (8.06), N = 4
	Before (N = 6)	0	388 (31)	0.36 (0.12)	0.16 (0.05)	50.0 (19.60), N = 2	
	After (N = 21)	2	394 (49)	0.38 (0.16)	0.30 (0.24)	55.3 (19.28), N = 9	81.0 (8.06), N = 4
	After WT (N = 19)		400 (45)	0.35 (0.14)	0.27 (0.23)		
Exp.	All (N = 7)	0	437 (48)	0.33 (0.12)	0.25 (0.15)	70.0 (24.49), N = 5	84.5 (3.84), N = 4
	$\|D\| < 1.5$ (N = 5)	0	422 (23)	0.26 (0.04)	0.22 (0.05)	82.0 (5.48), N = 4	
Mann-Whitney	Cont. WT versus Exp. All		0.0820	0.5522	0.6919		
U-test *p* values	Before versus Exp. All		0.0633	0.4751	0.3173		
	Before versus After WT		0.2794	0.7746	0.6332		

(A) Electrode position analysis results for each subject. The first 11 columns indicate the subject number (Sub.), ordered by date of surgery from earliest to most recent; the condition ("Cont" indicates control, and "Exp" indicates a custom insertion plan was used); the laterality ("Side"), where "L" indicates left ear and "R" indicates a right ear; the duration of hearing loss in years before implantation ("Dur HL"); the wear time in hours per day as measured using datalogging; age at implantation in years; age at testing in years; everyday hearing configuration, which was either unilateral implant ("Unil"), bilateral implant ("Bilat"), or bimodal ("Bimod"); whether the ear is the first implanted ear ("1st Ear"), with "N" indicating it was not the patients first implanted ear and "Y" indicating it was; Etiology of hearing loss, which was either unknown or due to noise, meningitis, Meneire's disease, Otosclerosis ("Otosler."), familial hearing loss, Auditory neuropathy spectrum disorder ("ANSD"), or Neurofibromatosis Type II ("NF2"); and biological sex, with "F" indicating female and "M" indicating male. The next five columns correspond to EL position metrics and are defined identically to Table 1. A column indicating folding was not included as there were no folded arrays in this dataset. The final two columns contain CNC word recognition scores recorded in the unilateral, implant only condition and in the bimodal condition, when available. (B) Summary statistics for each condition and group.

the actual depth was 1.7 mm shallower than the planned depth, and the resulting AID was 342 degrees, the shallowest insertion in the experimental group. With clinical subject 6, the first experimental case, we observe the base depth error to be 2.7 mm, corresponding to an over-insertion and the deepest observed AID of 542 degrees, well beyond the ideal 450 degrees for this EL. The base insertion depth for subject 12 was 2.2 mm shallower than the planned depth, leading to increased MMD in the most basal contacts of the array. As we did not observe any abnormalities with these patients or specimens, we hypothesize that this may be a limitation of text-based guidance in communicating clear and precise instructions on insertion depth. Large base depth errors can impact overall EL positioning, as observed in both this study and the previous one conducted with a different EL (18). This motivates the development of techniques to improve communication of the planned depth. Separate analyses were performed for all experimental cases, versus those where base depth was within 1.5 mm of the planned depth, which may indicate expected electrode placement if adherence to the planned depth can be improved in the future.

In the temporal bone specimen study, we found 0 of 7 experimental insertions folded or translocated. This is in contrast with the control insertions, for which 3 of 14 translocated (including 2 folded arrays). Array folding may lead to intracochlear trauma and worsened performance, often leading to the need for revision surgery (35). However, folding and translocation both tend to occur more frequently in temporal bone specimen insertions compared with clinical ones, likely due to degraded tissue integrity for ex vivo temporal bones (36). In the nonguided condition, we indeed observed higher translocation rates in the temporal bones than reported with the clinical use of this same device (37). Because translocation impacts AID, MMD, and AMD, and the clinical translocation rate with this electrode is relatively low (2 of 28 in the control group), we also compared EL position across groups after removing the folded and translocated array cases from the control group. Although no significant differences were identified with the Mann-Whitney *U* test in this relatively small study, there were trends toward lower AMD, MMD, and AID error. With preoperative planning, EL positioning within ST was observed in all cases.

We include analysis of the experimental with $|D| < 1.5$-mm group to observe EL positioning when the achieved depth is close to the plan. Given the current mean and standard deviation of the control WT and experimental with $|D| < 1.5$-mm groups, power analysis suggests that 14 experimental cases would be needed to have a power of 0.80 to detect a significant difference in AID at the $p < 0.05$ level with the Mann-Whitney *U* test. Sixty-six cases and 81 cases would be needed for similar power to detect differences in MMD and AMD. We found significantly reduced variability in MMD using the Brown-Forsythe test and a trend toward reduced variability in AID and AMD for the experimental with $|D| < 1.5$-mm group compared with controls. Reduced variability suggests that if the plan is successfully followed, EL positioning can become more standardized.

Using the pull-back technique, AMD was reduced without significant change in AID. Achieving reduced modiolar

TABLE 3. *Pooled EL position statistics across the temporal bone and clinical control WT and experimental groups*

Condition		AID (°)	MMD (mm)	AMD (mm)
Control WT		401 (41)	0.34 (0.13)	0.23 (0.19)
Exp. All (after pullback)		424 (43)	0.34 (0.09)	0.20 (0.12)
Exp. $\|D\| < 1.5$ mm		422 (19)	0.30 (0.07)	0.18 (0.06)
Mann-Whitney *U* test	Control all versus Exp. All	0.184	0.792	0.933
	Control all versus Exp. $\|D\| < 1.5$	0.141	0.315	0.932
Brown-Forsythe test	Control all versus Exp. All	0.610	0.181	0.352
	Control all versus Exp. $\|D\| < 1.5$	0.051	**0.039**	0.165

Significant *p* values are in bold.

distance at the apical portion of the array is of interest because channel interaction due to modiolar distance has been shown to have greater effect for apically located electrodes compared with basal electrodes (38–40).

We hypothesized that the use of the insertion planning approach may lead to learning effects for surgeons after using insertion planning. If substantial learning effects existed, then after using the planning tool for a series of cases, future EL placements should improve even without the use of preoperative planning. We observed no significant differences in the pre- or post-planning insertions. Further experiments are necessary to evaluate potential learning effects.

There are several limitations to this study. First, with limited sample size, there was limited statistical power. Also, there was limited ability to measure adherence to the insertion plan. Although it was possible to measure the final base insertion depth, it was not possible to measure the implemented insertion angles. This may be important as the previous study found that deviations intentionally introduced in the planned yaw angle were associated with scalar translocations and increased MMD, and deviated pitch angles were associated with increased AID error (18). Next, only one type of EL was evaluated in this study, although the method has also been validated with another precurved EL (18). Future work will be aimed at developing better strategies for communicating the plans to the surgeon as well as strategies for actively monitoring and providing feedback on the insertion, because final EL position is sensitive to successful plan implementation. Future experiments will also include multiple surgeons and increased sample size for both EL types. Although precurved ELs were the focus of these studies, the insertion planning approach could be applicable to straight ELs, with some modifications to the strategy for determining optimal vector and depth (41,42).

Of the seven subjects for whom insertion plans were used clinically, CNC word recognition test scores were available for five cases from at least 6 months post-implantation and were found to be 70.0 ± 24.49%. A larger sample size is necessary to confirm using insertion plans improves hearing outcomes; however, these results are consistent with multiple studies that have shown well positioned precurved arrays to be associated with significantly higher speech recognition performance (4,5,7,8,11).

CONCLUSIONS

Trends toward improved electrode array positioning within scala tympani were observed when electrode insertion plans are used. A larger sample size is necessary to statistically confirm that arrays are better positioned and hearing outcomes are improved when insertion plans are used. Variability in MMD was significantly reduced when the planned depth was achieved. Reduced variability suggests that if the plan is successfully followed, EL positioning can become more standardized. Relatively large differences between the planned and realized insertions depths were observed in 3 of 14 experiments where the plan was used. This motivates future work aimed at developing better strategies for communicating the plans to the surgeon as well as strategies for actively monitoring and providing feedback on adherence to the electrode insertion plan.

Acknowledgments: The temporal bones used in this study were purchased with support by the Robert H. Ossoff, D.M.D., M.D., Endowed Directorship for Translational Research in Otolaryngology in the Department of Otolaryngology–Head and Neck Surgery at Vanderbilt University Medical Center.

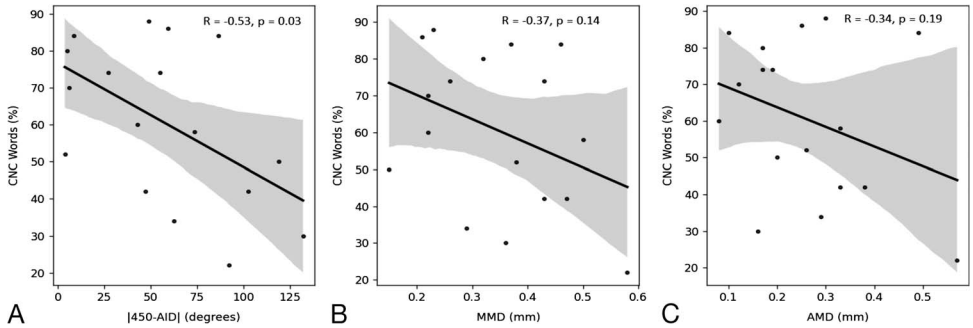

FIG. 3. Scatter plots of AID error on horizontal axis (*A*), MMD on horizontal axis (*B*), and AMD on horizontal axis (*C*) versus CNC word scores in the electric-only condition on the vertical axis. A regression line (black line) and 95% confidence interval (shaded area) are also shown in each plot.

REFERENCES

1. National Institute on Deafness and Other Communication Disorders. Available at: https://www.nidcd.nih.gov/sites/default/files/Documents/health/hearing/FactSheetCochlearImplant.pdf. Accessed May 10, 2022.
2. Boyer E, Karkas A, Attye A, et al. Scalar localization by cone-beam computed tomography of cochlear implant carriers: A comparative study between straight and periomodiolar precurved electrode arrays. *Otol Neurotol* 2015;36:422–9.
3. Gstoettner WK, Adunka O, Franz P, et al. Perimodiolar electrodes in cochlear implant surgery. *Acta Otolaryngol* 2001;121:216–9.
4. Holden LK, Finley CC, Firszt JB, et al. Factors affecting open-set word recognition in adults with cochlear implants. *Ear Hear* 2013;34:342–60.
5. Chakravorti S, Noble JH, Gifford RH, et al. Further evidence of the relationship between cochlear implant electrode positioning and hearing outcomes. *Otol Neurotol* 2019;40:617–24.
6. Davis TJ, Zhang D, Gifford RH, et al. Relationship between electrode-to-modiolus distance and current levels for adults with cochlear implants. *Otol Neurotol* 2016;37:31–7.
7. Carlson ML, Driscoll CL, Gifford RH, et al. Implications of minimizing trauma during conventional cochlear implantation. *Otol Neurotol* 2011;32:962–8.
8. Wanna GB, Noble JH, Gifford RH, et al. Impact of intrascalar electrode location, electrode type, and angular insertion depth on residual hearing in cochlear implant patients: preliminary results. *Otol Neurotol* 2015;36:1343–8.
9. Finley CC, Skinner MW. Role of electrode placement as a contributor to variability in cochlear implant outcomes. *Otol Neurotol* 2008;29:920–8.
10. Skinner MW, Ketten DR, Holden LK, et al. CT-derived estimation of cochlear morphology and electrode array position in relation to word recognition in nucleus-22 recipients. *J Assoc Res Otolaryngol* 2002;3:332–50.
11. Holder JT, Kessler DM, Noble JH, Gifford RH, Labadie RF. Prevalence of extracochlear electrodes: Computerized tomography scans, cochlear implant maps, and operative reports. *Otol Neurotol* 2018;39:e325–31.
12. Wanna GB, Noble JH, Carlson ML, et al. Impact of electrode design and surgical approach on scalar location and cochlear implant outcomes. *Laryngoscope* 2014;124(S6):S1–7.
13. Wang J, Dawant BM, Labadie RF, Noble JH. Retrospective evaluation of a technique for patient-customized placement of precurved cochlear implant electrode arrays. *Otolaryngol Head Neck Surg* 2017;157:107–12.
14. Ketten DR, Skinner MW, Wang GE, et al. In vivo measures of cochlear length and insertion depth of nucleus cochlear implant electrode arrays. *Ann Otol Rhinol Laryngol Suppl* 1998;175:1–16.
15. Erixon E, Högstorp H, Wadin K, Rask-Andersen H. Variational anatomy of the human cochlea: Implications for cochlear implantation. *Otol Neurotol* 2009;30:14–22.
16. Dimopoulos P, Muren C. Anatomic variations of the cochlea and relations to other temporal bone structures. *Acta Radiol* 1990;31:439–44.
17. Hardy M. The length of the organ of Corti in man. *Am J Anat* 1938;62:179–311.
18. Labadie RF, Noble JH. Preliminary results with image-guided cochlear implant insertion techniques. *Otol Neurotol* 2018;39:922–8.
19. Benson JC, Carlson ML, Lane JI. MRI of the internal auditory canal, labyrinth, and middle ear: How we do it. *Radiology* 2020;297:252–65.
20. Jun B, Song S. Surgical considerations during cochlear implantation: The utility of temporal bone computed tomography. *J Laryngol Otol* 2021;135:134–41.
21. Noble JH, Labadie RF, Majdani O, Dawant BM. Automatic segmentation of intra-cochlear anatomy in conventional CT. *IEEE Trans Biomedical Eng* 2011;58:2625–32.
22. Noble JH, Gifford RH, Labadie RF, Dawant BM. Statistical shape model segmentation and frequency mapping of cochlear implant stimulation targets in CT. *Med Image Comput Comput Assist Interv* 2012;15(Pt 2):421–8.
23. Wang J, Noble JH, Dawant BM. Metal artifact reduction for the segmentation of the intra cochlear anatomy in CT images of the ear with 3D-conditional GANs. *Med Image Anal* 2019;58:101553.
24. Helpard L, Li H, Rohani SA, et al. An approach for individualized cochlear frequency mapping determined from 3D synchrotron radiation phase-contrast imaging. *IEEE Trans Biomed Eng* 2021;68:3602–11.
25. Noble JH, Dawant BM, Warren FM, Labadie RF. Automatic identification and 3D rendering of temporal bone anatomy. *Otol Neurotol* 2009;30:436–42.
26. Noble JH, Warren FM, Labadie RF, Dawant BM. Automatic segmentation of the facial nerve and chorda tympani in CT images using spatially dependent feature values. *Med Phys* 2008;35:5375–84.
27. Peterson GE, Lehiste I. Revised CNC lists for auditory tests. *J Speech Hear Disord* 1962;27:62–70.
28. Riemann C, Sudhoff H, Todt I. The pull-back technique for the 532 slim modiolar electrode. *Biomed Res Int* 2019;2019:6917084.
29. Smetak MR, Riojas KE, Whittenbarger N, Noble JH, Labadie RF. Dynamic behavior and insertional forces of a precurved electrode using the pull-back technique in a fresh microdissected cochlea. *Otol Neurotol* 2023;44:324–30.
30. Zhao Y, Dawant BM, Labadie RF, Noble JH. Automatic localization of closely-spaced cochlear implant electrode arrays in clinical CTs. *Med Phys* 2018;45:5030–40.
31. Zhao Y, Chakravorti S, Labadie RF, Dawant BM, Noble JH. Automatic graph-based method for localization of cochlear implant electrode arrays in clinical CT with sub-voxel accuracy. *Med Image Anal* 2019;52:1–12.
32. Gifford RH, Shallop JK, Peterson AM. Speech recognition materials and ceiling effects: Considerations for cochlear implant programs. *Audiol Neurotol* 2008;13:193–205.
33. Dornhoffer JR, Reddy P, Meyer TA, et al. Individual differences in speech recognition changes after cochlear implantation. *JAMA Otolaryngol Head Neck Surg* 2021;147:280–6.
34. Beyea JA, McMullen KP, Harris MS, et al. Cochlear implants in adults: Effects of age and duration of deafness on speech recognition. *Otol Neurotol* 2016;37:1238–45.
35. Zuniga MG, Rivas A, Hedley-Williams A, et al. Tip fold-over in cochlear implantation: Case series. *Otol Neurotol* 2017;38:199–206.
36. Olson ES, Mountain DC. Mapping the cochlear partition's stiffness to its cellular architecture. *J Acoust Soc Am* 1994;95:395–400.
37. Durakovic N, Kallogjeri D, Wick CC, et al. Immediate and 1-year outcomes with a slim modiolar cochlear implant electrode array. *Otolaryngol Head Neck Surg* 2020;162:731–6.
38. Yang H, Won JH, Choi I, Woo J. A computational study to model the effect of electrode-to-auditory nerve fiber distance on spectral resolution in cochlear implant. *PLoS One* 2020;15:e0236784.
39. Briare JJ, Frijns JH. The consequences of neural degeneration regarding optimal cochlear implant position in scala tympani: A model approach. *Hear Res* 2006;214(1–2):17–27.
40. Frijns JH, Briaire JJ, Grote JJ. The importance of human cochlear anatomy for the results of modiolus-hugging multichannel cochlear implants. *Otol Neurotol* 2001;22:340–9.
41. Khan MMR, Labadie RF, Noble JH. Preoperative prediction of angular insertion depth of lateral wall cochlear implant electrode arrays. *J Med Imaging (Bellingham)* 2020;7:031504.
42. Rivas A, Cakir A, Hunter JB, et al. Automatic cochlear duct length estimation for selection of cochlear implant electrode arrays. *Otol Neurotol* 2017;38:339–46.
43. Stakhovskaya O, Sridhar D, Bonham BH, Leake PA. Frequency map for the human cochlear spiral ganglion: Implications for cochlear implants. *J Assoc Res Otolaryngol* 2007;8:220–33.
44. Buss E, Pillsbury HC, Buchman CA, et al. Multicenter US bilateral MED-EL cochlear implantation study: Speech perception over the first year of use. *Ear Hear* 2008;29:20–32.
45. Dorman MF, Yost WA, Wilson BS, Gifford RH. Speech perception and sound localization by adults with bilateral cochlear implants. *Semin Hear* 2011;32:073–89.
46. Gifford RH, Dorman MF, Sheffield SW, Teece K, Olund AP. Availability of binaural cues for bilateral implant recipients and bimodal listeners with and without preserved hearing in the implanted ear. *Audiol Neurotol* 2014;19:57–71.
47. Litovsky R, Parkinson A, Arcaroli J, Sammeth C. Simultaneous bilateral cochlear implantation in adults: A multicenter clinical study. *Ear Hear* 2006;27:714–31.
48. de Brito R, Bittencourt AG, Goffi-Gomez MV, et al. Cochlear implants and bacterial meningitis: A speech recognition study in paired samples. *Int Arch Otorhinolaryngol* 2013;17:57–61.